Second harmonic spectroscopy of surface lattice resonances

Journal:	*Nano Letters*
Manuscript ID	nl-2018-03574g.R1
Manuscript Type:	Communication
Date Submitted by the Author:	29-Nov-2018
Complete List of Authors:	Hooper, David; University of Bath, Department of Physics Kuppe, Christian ; University of Bath, Department of Physics Wang, Danqing; Northwestern University, Applied Physics Wang, Weijia; Northwestern University, Guan, Jun; Northwestern University, Applied Physics Odom, Teri; Northwestern University, Chemistry; Northwestern University, Chemistry Valev, Ventsislav; University of Bath, Physics

Second harmonic spectroscopy of surface lattice resonances

*David C. Hooper[1], Christian Kuppe[1], Danqing Wang[2], Weijia Wang[2], Jun Guan[2], Teri W. Odom[2,3,4] and Ventsislav K. Valev[1]**

[1]Centre for Photonics and Photonic Materials and Centre for Nanoscience and Nanotechnology, Department of Physics, University of Bath, Claverton Down, Bath, BA2 4JY, UK

[2]Graduate Program in Applied Physics, Northwestern University, Evanston, Illinois, 60208, USA

[3]Department of Materials Science and Engineering, Northwestern University, Evanston, Illinois, 60208, USA

[4]Department of Chemistry, Northwestern University, Evanston, Illinois, 60208, USA

KEYWORDS Nonlinear optics, Plasmonics, Quadrupoles, Surface lattice resonance

ABSTRACT

Because of their large figures of merit, surface lattice resonances (SLRs) in metal nanoparticle arrays are very promising for chemical and biomolecular sensing, in both liquid and gas media. SLRs are sensitive to refractive index changes both near the surface of the nanoparticles (surface sensitivity) and in the volume between them (bulk sensitivity). Due to its intrinsic surface-sensitivity and a power-law dependence on electric fields, second harmonic generation (SHG) spectroscopy can improve upon both the surface and volume sensitivities of SLRs. In this report on SHG spectroscopy of plasmonic nanoparticles, we show that the SHG signal is greatly increased (up to 450 times) by the SLRs. We also demonstrate very narrow resonances in SHG intensity (~5 nm FWHM). We illustrate how the SHG resonances are highly sensitive to SLRs by varying the fundamental wavelength, angle of incidence, nanoparticle material and lattice constant of the arrays. Finally, we identify an SHG resonance (10 nm FWHM) that is electric dipole forbidden and can be attributed to higher-order multipoles, enhanced by the strong near-fields of SLRs. Our results open up new and very promising avenues for chemical and biomolecular sensing, based on SHG spectroscopy of SLRs.

TEXT

Recently, nonlinear plasmonics has attracted significant research interest.[1,2] The reason is that nonlinear optical effects scale as a power law of the incident light and plasmonic nanostructures strongly concentrate the incident light into optical near-field “hotspots”. As a consequence, within such hotspots, nonlinear plasmonic effects are tremendously enlarged, offering prospects for new and improved applications.

Because nonlinear optical effects find applications in tuning laser light, significant research interest has been devoted to nanostructure-enhanced frequency conversion, with increasing efficiency. Various strategies have been employed for enhancing frequency conversion, such as using all-dielectric nanostructures for increased damage threshld,[3–5] plasmonic-dielectric hybrids where a plasmonic resonance enhances the frequency conversion of the dielectric,[6–8] and plasmonic nanostructures.[1,2,9] Nonlinear optical effects also find applications in multiphoton microscopy, useful for biological sciences and material characterization.[10] Plasmonic nanoparticles have thus been the subject of numerous investigations with second harmonic generation (SHG),[11–13] third harmonic generation,[14,15] and two-photon luminescence microscopy, to name just a few. Due to the frequency conversion, the measured signal in all these techniques is background free (from the illumination). The improved frequency conversion offered by plasmons can allow imaging with lower laser power and reduced photodamage to specimens (organic or inorganic).[16,17] The absence of signal background is also a key factor for the strong sensitivity of nonlinear optical effects, such as SHG chiral optical effects,[18–21] or magnetization-induced SHG[22,23] compared to their linear optical counterparts.[24] Though considerable attention has been devoted to the SHG enhancements from localized surface plasmons (LSPR) and metasurfaces,[25–31] surface lattice resonances (SLR)[32–36] have received much less consideration.[37,38]

SLRs are more promising for sensing applications than LSPRs because of their significantly narrower resonance linewidth (< 5 nm).[34,39–41] Since the resonance wavelength depends on the refractive index of the environment,[42] surface plasmons can be used for chemical and

biological sensing, in both liquid and gaseous media. Whereas for LSPRs the figure of merit (FoM) is typically on the order of a few units, for SLRs it is much larger,[43,44] (by one[45] and even two[46] orders of magnitude) and the narrower resonance linewidth is attributed to a Fano-type effect.[47] SLRs occur on plasmonic nanoparticles, arranged periodically, with a lattice constant of the order of the wavelength of incident light. The two determining factors for the SLR are the LSPR and the Rayleigh Anomaly (where light is diffracted in the plane of the array).[47–49] Specifically, the SLRs result from the coupling of the broad LSPR with the narrow frequency of the Rayleigh Anomaly, and hence exhibit a dual sensitivity – surface (on the nanoparticles) and bulk (between the nanoparticles).[50]

Here, we demonstrate SHG spectroscopy of SLRs, where the SHG signal is enhanced up to 450 times by SLRs; much above the previous reports of 10 and 30 times increase.[37,38] The measured SHG resonances can be as sharp as 5 nm in FWHM, which is promising for sensing. Indeed, we show that the SHG signal is very sensitive to the factors determining SLRs; we successfully tuned the SHG by varying the fundamental wavelength, the angle of incidence, the lattice parameter and the nanoparticle material. Importantly, we discover SHG spectroscopy resonances (10 nm FWHM) that are not associated with electric dipoles. We attribute these resonances to higher-order contributions, enhanced by the SLRs. For individual nanoparticles with diameter > 100 nm, retardation effects lead to higher-order terms (quadrupoles,[51] octupoles, etc.[52–55]), at the second harmonic frequency.[56,57] Whereas in previous decades, such higher-order contributions did not play a major role in material

properties, recent progress in nanofabrication has pushed them to the forefront of nonlinear plasmonics.[58,59]

We study four samples, where gold and silver plasmonic nanoparticles are arranged into two square lattices each, with periodicities: 580 nm and 600 nm. Further specifications of the samples can be found in section **S.1** of the supporting information. The sample geometry is shown in **Fig. 1a**. The nanoparticle arrays are fabricated using PEEL (a combination of photolithography, e-beam deposition, etching and lift-off). A scanning electron micrograph (SEM) of the 600 nm period array is shown in Fig. 1b. An advantage of this fabrication technique is the ability to create large-area (cm^2) uniform arrays, as demonstrated in Fig. 1c, where the nanoparticle array appears green, due to its diffractive properties. The linear transmission spectra as a function of the angle of incidence for the 600 nm period gold array are shown in Fig 1d, revealing the location of the SLR band edges. The Rayleigh anomaly dispersion, denoted by the green lines in Fig. 1d, is calculated using,[37]

$$\lambda_{(i,0)} = a_0\left(\frac{n}{|i|} - \frac{\sin(\theta)}{i}\right), \qquad (1.2)$$

where a_0 is the lattice periodicity, n is the refractive index of the surrounding environment, θ is the angle of incident, and i is an integer denoting the diffraction order. At the wavelength of the Rayleigh anomaly, the diffracted wave travels across the sample surface interacting with multiple nanoparticles. When the wavelength undergoing a Rayleigh anomaly interferes with the broad LSPR of individual nanoparticles, a Fano-type SLR occurs (**Fig. 2a**).

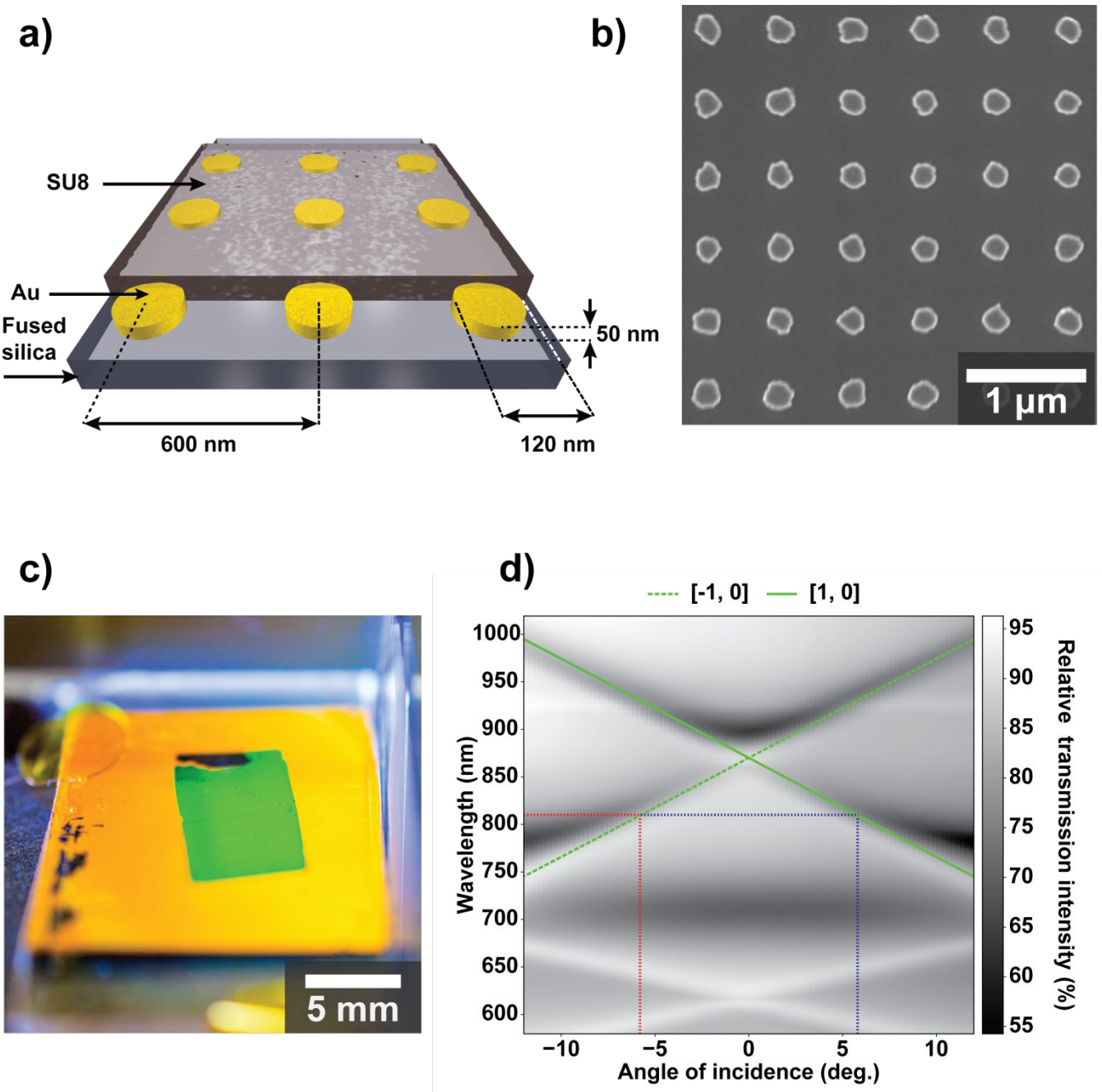

Figure 1. Our large-area gold nanoparticle arrays exhibit clear surface lattice resonances. a) Sample schematic and dimensions showing gold nanoparticles on a fused silica substrate and capped with photoresist (SU8). b) Scanning electron micrograph of the fabricated nanoparticle array before capping with SU8. c) Photograph of an investigated sample, the large-area nanostructured array appears green. d) Experimental mapping of transmission spectra versus

changing angle of incidence, upon illumination with vertically polarized light (S_{IN}). The green lines show theoretical calculations of the diffraction beams that couple into surface lattice resonances. The red and blue dashed lines indicate the angles of incidence for enhancing 810 nm fundamental light.

Fig. 2a shows a numerically calculated transmission spectrum (performed using Lumerical[60]) of the 600 nm period gold nanoparticle array, for normal incident light. The dip in transmission at 675 nm is attributable to the LSPR. The Rayleigh anomaly is at 870 nm and the SLR is at 872 nm. To illustrate the specific electromagnetic behavior of the SLR, we plot the results of numerical simulations at two different wavelengths – at the SLR and away from it. Specifically, these are electric field simulations, at the surface of a single nanoparticle, with periodic boundary conditions. In Fig. 2b, at 780 nm, i.e. away from the SLR, the electric field is concentrated around the nanoparticle. By contrast, in Fig. 2c, at 872 nm, i.e. at the wavelength of SLR, the electric field radiated by the nanoparticle extends to neighboring nanoparticles. This is evidenced by the electromagnetic radiation from the dipole reaching beyond a single unit cell. The enhancement of the electric near-field at the SLR leads to an increased SHG signal.

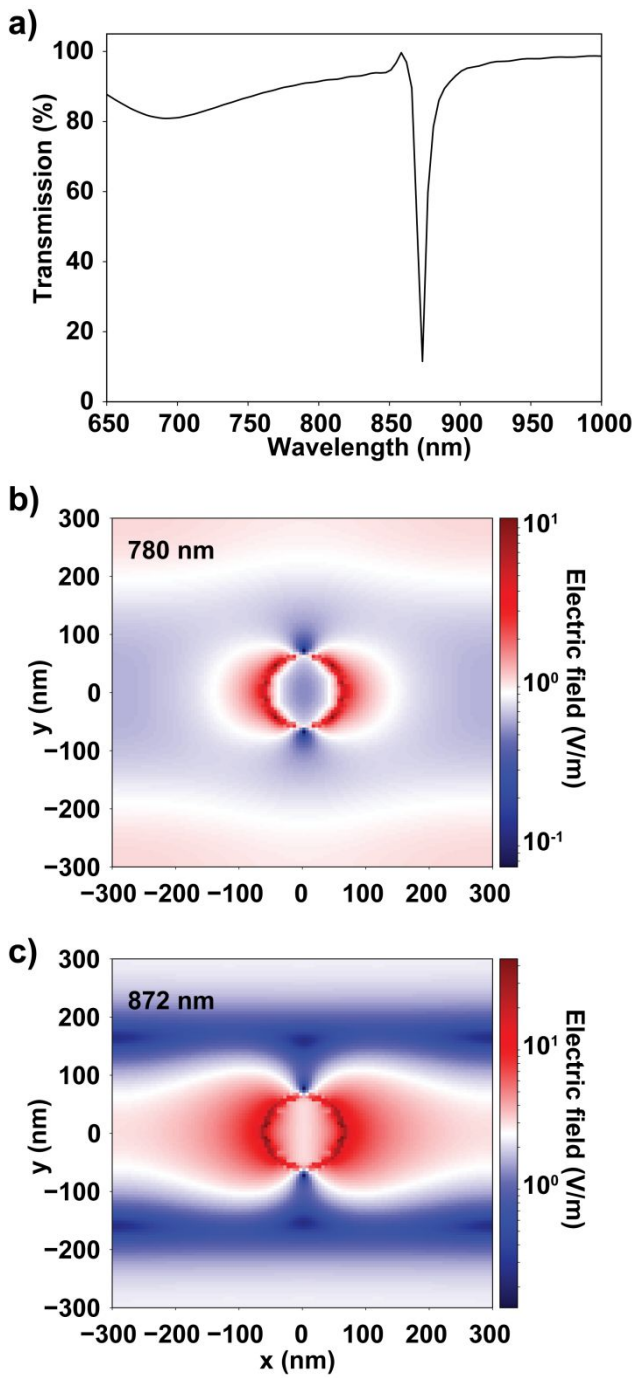

Figure 2. Numerical simulations illustrating the surface lattice resonance (SLR) enhancement of near-fields. a) For the 600 nm period gold array, the transmission at normal incidence clearly displays an SLR, at 872 nm. b) The electric near-field at the surface of the nanoparticle, away from resonance at 780 nm. c) The electric near-field at the surface of the nanoparticle, at 872

nm, the wavelength of SLR. A distinctive radiative dipole can be seen, illustrating the nature of the SLR.

Second harmonic generation is caused by a part of the material polarization that occurs and radiates at 2ω, i.e. twice the fundamental driving frequency ω. The total effective second order nonlinear polarization can be expressed as,

$$\mathbf{P}(2\omega) = \mathbf{P}^{D}(2\omega) + \mathbf{P}^{Q}(2\omega), \qquad (1.3)$$

where $\mathbf{P}^{D}(2\omega)$ is the dipole contribution to the second harmonic polarization, and $\mathbf{P}^{Q}(2\omega)$ represents the contribution from quadrupoles. These two terms can then be written in full as,[61]

$$\begin{aligned} P_i^{D}(2\omega) &= \chi_{ijk}^{(2,D)} E_j(\omega) E_k(\omega), \\ P_i^{Q}(2\omega) &= \chi_{ijkl}^{(2,Q)} E_j(\omega) \nabla_k E_l(\omega), \end{aligned} \qquad (1.4)$$

where summation over repeated indices is implied. The indices *i*, *j*, and *k*, take the Cartesian directions and $E(\omega)$ is the electric field of the incident light. Here, $\chi_{ijk}^{(2,D)}$ is a rank three tensor denoting the electric dipole susceptibility at the second harmonic, the first index designates the direction of the polarization and the final two indices are the directions of the input fields. The quadrupolar contribution is represented by the rank four tensor $\chi_{ijkl}^{(2,Q)}$. The expression for $P_i^{Q}(2\omega)$ in Equation 1.3 is obtained by a Taylor expansion and represents the quadrupolar contribution to the second order polarization, see section **S.2** in the supporting information for further details. Electric dipole contributions to SHG are forbidden in systems with inversion symmetry. Our arrays of gold nanoparticles possess C_{4v} symmetry and the corresponding $\chi_{ijk}^{(2,D)}$ tensor is[62]

$$\chi_{ijk}^{(2,D)} = \begin{pmatrix} 0 & 0 & 0 & 0 & \chi_{XXZ} & 0 \\ 0 & 0 & 0 & \chi_{XXZ} & 0 & 0 \\ \chi_{ZYY} & \chi_{ZYY} & \chi_{ZZZ} & 0 & 0 & 0 \end{pmatrix}. \quad (1.5)$$

This C_{4v} tensor is mathematically identical to the rotationally isotropic surface tensor. Equation 1.3 shows that the dipolar contribution to SHG scales as a power law of the electric field of incident light and that the quadrupolar contribution is proportional to gradients of that electric field. Notably, in SLRs, the bulk and surface sensitivities are characterized by a long-range radiative dipole coupling (which scales as e^{ikr}/r) and by a short-range electric near-field (which scales as $1/r^3$ and is characterized by strong electric field gradients), respectively. In other terms, on the one hand, SLRs are surface-sensitive: a spectral shift is induced in response to the refractive index change in the local environment. On the other hand, they are bulk-sensitive: the electromagnetic field of SLR modes is not confined to the plane of the array, it extends over a volume, tens of hundreds of nm across.[63,64] Consequently, combining SLRs and SHG presents obvious advantages and SHG spectroscopy of SLRs is currently of increasing interest.[37,38,65]

Our experiments demonstrate two types of SHG enhancement mechanism: one dominated by dipolar contribution (sensitive to the amplitude of SLR enhanced near-fields) and one dominated by higher-order contributions (additionally sensitive to the gradients of SLR enhanced near-fields). The SHG experimental set up is shown in **Fig. 3a**. A tunable femtosecond pulsed laser provides the incident fundamental wavelength which is adjusted to a power of 0.5 mW, the sample is mounted on an automated rotation stage to change the angle

of optical incidence, and an analyzing polarizer is used to decompose the SHG signal into its vertically (S) and horizontally (P) polarized components. See section **S.3** in the supporting information for further experimental details.

First, it is important to establish that the measurements clearly correspond to SHG; for instance, three-photon luminescence could spectrally overlap with the detected SHG signal. Previous studies did not report such a check.[37,38] To characterize the respective contributions from multiphoton luminescence and SHG, a series of bandpass filters are used, see Fig. 3b inset. The filters are centered at 10 nm intervals, with 10 nm FWHM. In this experiment, the fundamental wavelength and the angle of incidence are kept constant at 780 nm and 9.2°, respectively. These values are close to an SLR in the 600 nm period sample. As Fig. 3b illustrates, the strongest signal occurs at 390 nm, which is the SHG. For wavelengths 380 nm and below, as well as for wavelengths 400 nm and above, there is negligible signal, establishing that there is no contribution from multiphoton luminescence. The results unambiguously demonstrate that the signals we measure correspond to pure SHG.

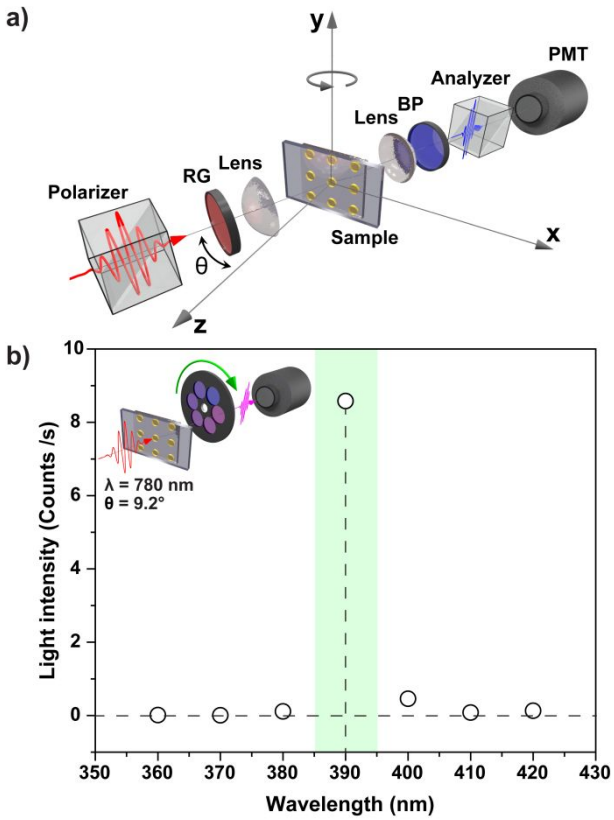

Figure 3. The second harmonic generation signal clearly stands out from the multiphoton background. a) Experimental configuration for the SHG measurements, where θ is the angle of incidence, RG is an RG665 Schott glass filter, BP is bandpass filter and, PMT is a photomultiplier tube. b) For illumination with 780 nm fundamental light, the multiphoton emission is plotted versus wavelength. A 10 nm FWHM bandpass filter was used for each detection wavelength, as indicated by the inset. The dashed vertical line shows the SHG signal and the shaded region shows the FWHM of the bandpass filter.

The SHG signal is greatly enhanced by the SLRs. We begin with the 600 nm period array of gold nanoparticles, illuminated at 810 nm. In **Fig. 4a**, the SHG intensity is plotted as a function of the angle of incidence, for the S_{IN}-P_{OUT} polarizer-analyzer configuration (i.e. vertical-in

horizontal-out). Two strong SHG enhancements are observed at around ± 6° angle of incidence. The red and green dashed lines in Fig. 1d correspond to the calculated Rayleigh anomalies at ± 5.7°, which are shown by the black dashed lines in Fig. 4a. For angles of incidence in between the peaks, there is no enhancement of SHG and the signal is below 0.2 counts per second. From these data, the SHG enhancement in the SLR peaks is over 150 times, due to the strong electric near-fields around the nanoparticles provided by the SLR. Notably, this enhancement is already much greater compared to the previous reports of 10 and 30 times,[37,38] but it can be even greater.

Next, we examine how the SLR enhancement of SHG is affected by fundamental wavelength, angle of incidence, array periodicity and nanoparticle material, see Fig. 4b, 4c, and 4d. Specifically, nanoparticle arrays with periodicities of 600 nm and 580 nm are investigated, and four fundamental wavelengths are used, throughout various angles of incidence. For each fundamental wavelength and each sample periodicity, there is a corresponding peak in SHG versus angle of incidence. The figures show that, as the fundamental wavelength is decreased, the corresponding SHG enhancement shifts to greater angles of incidence. The SHG peaks track the angle of incidence at which a corresponding SLR occurs. Between Fig. 4b and Fig. 4c, the peaks are offset in angle of incidence. This offset is due to the change in array periodicity, which affects the position of the SLRs. It should be noted that all our sample arrays are covered with SU8, and that the difference in their behavior is therefore not due to differences in their refractive index environment. Moreover, because

the azimuthal angle orientation of the arrays affects the dispersion of the Rayleigh anomalies, all samples were orientated with their lattice vectors parallel to the incident polarization.

Furthermore, we investigate silver nanoparticle arrays, with identical periodicities to those of the gold nanoarrays: 600 nm and 580 nm. In the case of silver, an SHG enhancement of up to 450 times is observed, for the 600 nm period array, as shown in Fig 4d. This enhancement occurs for a fundamental wavelength of 760 nm, at 11.2° angle of incidence (indicated with blue lines in **Fig. S1** of the supporting information). The strength of this SHG enhancement can be attributed to a strong SLR. Indeed, the SHG intensity scales as the 4th power of the electric near-fields, which are enhanced at the SLR. In Fig. S1, the deep black color near the intersection of the blue lines clearly indicates very low transmission through the arrays, i.e. a strong SLR.

At maximum enhancement an SHG conversion efficiency of $\eta_{SHG} = 1.5 \times 10^{-9}$ is obtained, where $\eta_{SHG} = P(2\omega)/P(\omega)$ with $P(2\omega)$ and $P(\omega)$ being the power of the SHG and fundamental, respectively. Here, SHG enhanced by SLRs results in conversion efficiencies comparable to previous studies on plasmonic nanostructures.[66–68] Structures explicitly designed for efficient SHG can achieve much higher conversion efficiencies.[69] However, for sensing applications the conversion efficiency is not the most crucial factor. Rather, it is the relative contrast in SHG that is important. Therefore, SLRs provide an appealing platform for sensing given the dramatic variation in SHG between on and off resonance demonstrated in this work.

In both Fig. 3 and Fig. 4, the SHG signal is electric dipole allowed. The experimental geometries (polarizer-analyzer combinations and angles of optical incidence) address the non-zero tensor elements in Equation 1.4. In order to evidence the higher-order contributions to SHG, we must select an experimental geometry that is electric dipole forbidden, i.e. one which addresses a zero tensor component in Equation 1.4.

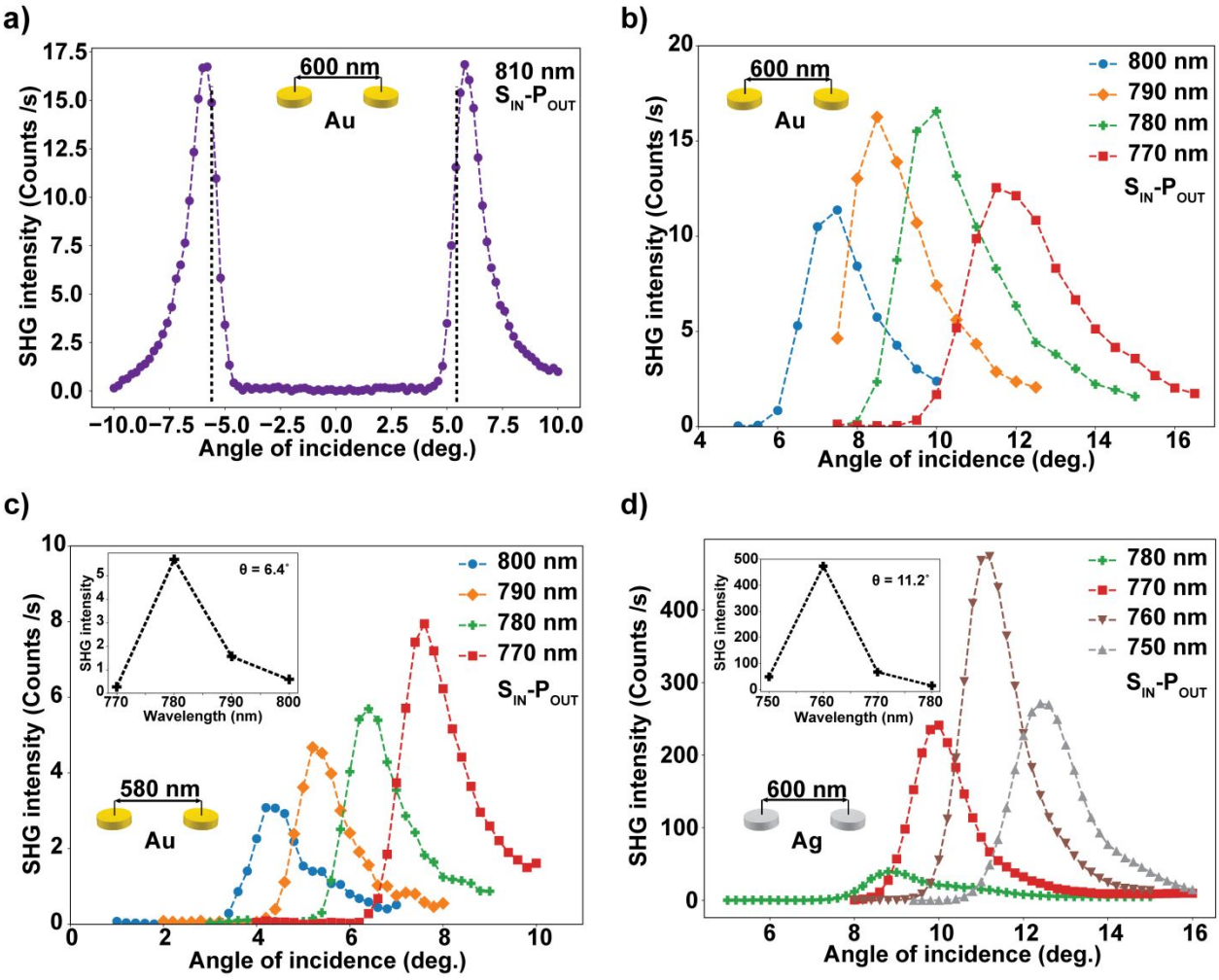

Figure 4. Due to the strong near-fields of SLRs, SHG enhancements (up to 450 times) occur by tuning fundamental wavelength, angle of incidence and lattice constant of the arrays. a) SHG enhancement from an SLR occurs near the Rayleigh anomaly corresponding to the

fundamental wavelength of 810 nm for the 600 nm period array. Enhancement occurs symmetrically for positive and negative angles of incidence. The 810 nm wavelength corresponds to the red and blue lines in Fig. 1d. b) and c) enhanced SHG at different fundamental wavelengths for the 600 nm and 580 nm period gold nanoparticle arrays, respectively. d) enhanced SHG at different fundamental wavelengths for the 600 nm period silver nanoparticle array. The strong enhancements follow the angles of incidence that correspond to a Rayleigh anomaly induced SLR at the fundamental wavelength. The insets in (c) and (d) show the SHG intensity for different fundamental wavelengths at a single angle of incidence. All data acquired in the vertical-horizontal polarizer-analyzer configuration.

In **Fig. 5**, we demonstrate the SLR enhancement of the higher-order contributions to SHG. Here, the experimental geometry of interest is the S_{IN}-S_{OUT} (vertical-vertical) polarizer-analyzer configuration, at normal incidence. Under these conditions, within the electric dipole tensor, only the χ_{YYY} tensor component is addressed. As we can see in Equation 1.4, this component is zero, for our samples, i.e. SHG is from electric dipoles is forbidden. Fig. 5a shows the SHG signal versus the angle of incidence, for a fundamental wavelength of 870 nm incident on the 600 nm period gold nanoparticle array. For the S_{IN}-S_{OUT} (vertical-vertical) polarizer-analyzer configuration, a distinct SHG peak can be seen (orange diamonds), centered at normal incidence, i.e. precisely in the electric dipole forbidden configuration. This enhancement is attributable to the SLR near normal incidence. Indeed, 870 nm is very close to the normal incidence SLR, as demonstrated by both theory and experiment. Numerically, we calculate the

SLR position at 872 nm, see Fig. 2c. Experimentally, in the S_{IN}-P_{OUT} (vertical-horizontal) polarizer-analyzer configuration, which is electric dipole allowed, we observe two peaks (blue dots) that are similar to the data in Fig. 4a and are only 2° apart in angle of incidence.

Additionally, Fig. 5b unambiguously demonstrates that the SHG enhancement in the electric dipole forbidden configuration is due to the normal incidence SLR. The data were recorded for both gold nanoparticle samples, in the S_{IN}-S_{OUT} (vertical-vertical) polarizer-analyzer configuration and at normal incidence, see section **S.2** of the supporting information for further details. For each sample, the SHG spectra peak (10 nm FWHM) is at the wavelengths of SLR, red-shifted with respect to the wavelength of Rayleigh anomaly.

Physically, there is a direct link between SLRs and the higher-order contributions to SHG. First, to avoid confusion, we point out that we do not discuss plasmonic quadrupolar modes in the nanoparticle. As can be seen from equation 1.3, the quadrupolar contribution to the second harmonic polarization is proportional to gradients of the local electric field. At the SLR, such gradients of the local electric fields are very strongly pronounced, see Fig. 2c. It should be pointed out that quadrupolar SHG can originate from the surface of the nanoparticles.[70]

Our analysis of the SHG results in Fig. 5 is based on the assumption that we address the zero tensor component in Equation 1.4, which implies 4-fold (or isotropic) symmetry. However, small shape imperfections of the nanostructures can break the isotropy leading to the appearance of electric dipole allowed SHG at normal incidence.[71,72] Moreover, lattice defects could also lead to electric dipole allowed SHG. These hypothetical electric dipole contributions would usually be very small but, in our experiments, they could be enhanced by the SLRs and

become measurable. However, as can be seen in Fig 5a, the SHG signal for S_{IN}-S_{OUT} peaks at normal incidence and not at the angles corresponding to the SRLs, where electric dipole SHG attributable to surface lattice resonantly-enhanced imperfections should have appeared (±1°). Therefore, the S_{IN}-S_{OUT} signal cannot be attributed to an SLR enhanced electric dipolar contribution to SHG.

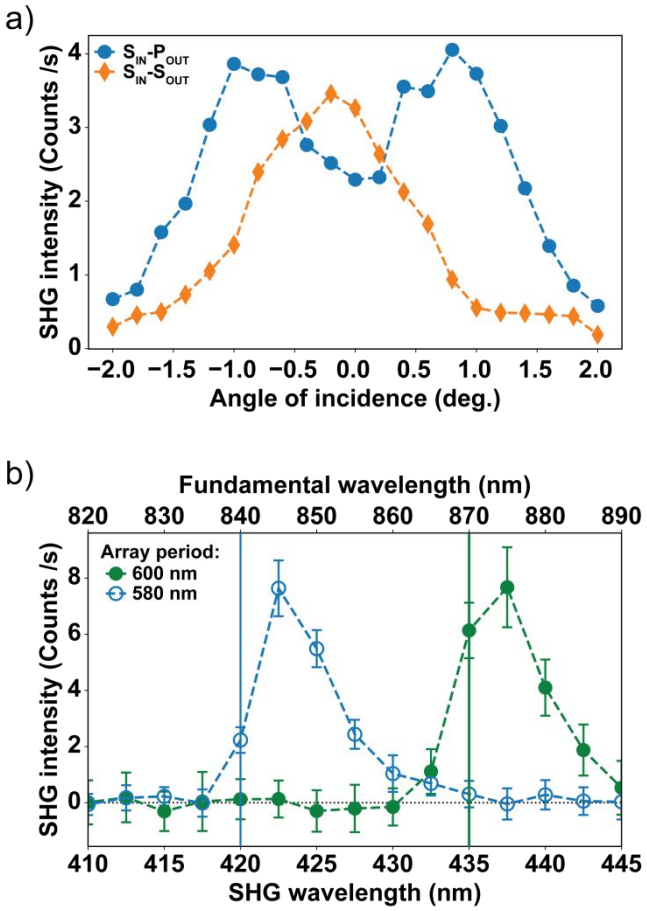

Figure 5. SLR causes an enhancement of the SHG quadrupolar contributions for the gold arrays. a) For S_{IN}-P_{OUT} (dots) the SHG signal is attributable to electric dipolar contributions. The fundamental light is at 870 nm (at the Rayleigh anomaly) and the peaks correspond to the SLRs. For S_{IN}-S_{OUT} (diamonds), the signal peaks at normal incidence, where the higher-order

contributions to SHG appear. b) Measuring SHG spectra, for S_{IN}-S_{OUT} and at normal incidence, these higher-order contributions to SHG peak at the normal incidence SLR wavelength, for both the 600 nm and 580 nm period arrays. The blue and green solid lines indicate the Rayleigh anomalies for the 580 and 600 nm periodicities, respectively. Error bars represent the standard deviation from the mean average counts.

In conclusion, we demonstrate SHG spectroscopy from SLRs, where the signal can be enhanced up to 450 times. We present both electric-dipole allowed (in Fig. 4) and electric-dipole forbidden (in Fig. 5) SHG resonances. We observe SHG resonances as narrow as 5 nm FWHM, which indicates that a high FoM can be achieved, opening new avenues for chemical and biosensing applications. Moreover, the SHG technique is intrinsically surface-sensitive, which can lead to improved near-field surface sensing, especially using higher-order resonances that originate from gradients in plasmonic near-fields, see equation 1.3. Equation 1.3 also demonstrates how SHG can improve upon the bulk sensitivity of SLRs. This bulk sensitivity originates from far-field coupling between nanoparticles and, for electric dipole allowed SHG resonances, the sensitivity would additionally benefit from a power law dependence on the far-fields. It should also be pointed out that the SHG process occurs via virtual energy levels at ultrafast timescales.[62] This process could therefore enable ultrafast probes of the refractive index and could be useful for monitoring chemical reactions, e.g. catalysis by the nanoparticles. To explore the limits of these applications, future work should focus on the importance of the environment surrounding the nanoparticle arrays.[73,74]

ASSOCIATED CONTENT

Supporting Information

Supporting Information contains details on (i) sample specifications, (ii) higher order contributions to SHG, (iii) experimental details, (iv) results for silver nanoparticle arrays, and (v) power dependence measurement (PDF)

AUTHOR INFORMATION

Corresponding Author
*v.k.valev@bath.ac.uk

ORCID
Danqing Wang: 0000-0002-7369-1944
Teri W. Odom: 0000-0002-8490-292X
David C. Hooper: 0000-0002-2259-6592
Ventsislav K. Valev: 0000-0001-9951-1836
Christian Kuppe: 0000-0002-7562-8789

Author Contributions

The manuscript was written through contributions from all authors. All authors have given approval to the final version of the manuscript. T.O. and V.K.V. designed the research. D.W., J.G. and W.W. prepared the samples. D.C.H. performed the SHG experiments. C.K. and D.W. conducted numerical simulations. D.C.H. and V.K.V. analyzed the results. D.C.H. and V.K.V. wrote the first draft of the paper and all authors contributed to the final text.

ACKNOWLEDGMENT

VKV acknowledges support from the Royal Society through the University Research Fellowships. We acknowledge Royal Society grants CHG\R1\170067, PEF1\170015 and RGF\EA\180228, as well as STFC ST/R005842/1. DCH acknowledges funding and support from the Engineering and Physical Sciences Research Council (EPSRC) Centre for Doctoral Training in Condensed Matter Physics (CDTCMP), Grant No. EP/L015544/1. This work was also supported by the Vannevar Bush Faculty Fellowship from DOD under N00014-17-1-3023 (T.W.O.).

Notes

The authors declare no competing financial interest.

REFERENCES

(1) Kauranen, M.; Zayats, A. V. Nonlinear Plasmonics. *Nat. Photonics* **2012**, *6* (11), 737–748. https://doi.org/10.1038/nphoton.2012.244.

(2) Butet, J.; Brevet, P.-F.; Martin, O. J. F. Optical Second Harmonic Generation in Plasmonic Nanostructures: From Fundamental Principles to Advanced Applications. *ACS Nano* **2015**, *9* (11), 10545–10562. https://doi.org/10.1021/acsnano.5b04373.

(3) Liu, S.; Vabishchevich, P. P.; Vaskin, A.; Reno, J. L.; Keeler, G. A.; Sinclair, M. B.; Staude, I.; Brener, I. An All-Dielectric Metasurface as a Broadband Optical Frequency Mixer. *Nat. Commun.* **2018**, *9* (1), 2507–2512. https://doi.org/10.1038/s41467-018-04944-9.

(4) Semmlinger, M.; Tseng, M. L.; Yang, J.; Zhang, M.; Zhang, C.; Tsai, W. Y.; Tsai, D. P.; Nordlander, P.; Halas, N. J. Vacuum Ultraviolet Light-Generating Metasurface. *Nano Lett.* **2018**, *18* (9), 5738–5743. https://doi.org/10.1021/acs.nanolett.8b02346.

(5) Shcherbakov, M. R.; Neshev, D. N.; Hopkins, B.; Shorokhov, A. S.; Staude, I.; Melik-Gaykazyan, E. V.; Decker, M.; Ezhov, A. A.; Miroshnichenko, A. E.; Brener, I.; et al. Enhanced Third-Harmonic Generation in Silicon Nanoparticles Driven by Magnetic Response. *Nano Lett.* **2014**, *14* (11), 6488–6492. https://doi.org/10.1021/nl503029j.

(6) Aouani, H.; Rahmani, M.; Navarro-Cía, M.; Maier, S. A. Third-Harmonic-Upconversion Enhancement from a Single Semiconductor Nanoparticle Coupled to a Plasmonic Antenna. *Nat. Nanotechnol.* **2014**, *9* (4), 290–294.

https://doi.org/10.1038/nnano.2014.27.

(7) Timpu, F.; Hendricks, N. R.; Petrov, M.; Ni, S.; Renaut, C.; Wolf, H.; Isa, L.; Kivshar, Y.; Grange, R. Enhanced Second-Harmonic Generation from Sequential Capillarity-Assisted Particle Assembly of Hybrid Nanodimers. *Nano Lett.* **2017**, *17* (9), 5381–5388. https://doi.org/10.1021/acs.nanolett.7b01940.

(8) Shibanuma, T.; Grinblat, G.; Albella, P.; Maier, S. A. Efficient Third Harmonic Generation from Metal-Dielectric Hybrid Nanoantennas. *Nano Lett.* **2017**, *17* (4), 2647–2651. https://doi.org/10.1021/acs.nanolett.7b00462.

(9) Fan, W.; Zhang, S.; Panoiu, N. C.; Abdenour, A.; Krishna, S.; Osgood, R. M.; Malloy, K. J.; Brueck, S. R. J. Second Harmonic Generation from a Nanopatterned Isotropic Nonlinear Material. *Nano Lett.* **2006**, *6* (5), 1027–1030. https://doi.org/10.1021/nl0604457.

(10) Berweger, S.; Atkin, J. M.; Xu, X. G.; Olmon, R. L.; Raschke, M. B. Femtosecond Nanofocusing with Full Optical Waveform Control. *Nano Lett.* **2011**, *11* (10), 4309–4313. https://doi.org/10.1021/nl2023299.

(11) Valev, V. K.; Smisdom, N.; Silhanek, A. V.; De Clercq, B.; Gillijns, W.; Ameloot, M.; Moshchalkov, V. V.; Verbiest, T. Plasmonic Ratchet Wheels: Switching Circular Dichroism by Arranging Chiral Nanostructures. *Nano Lett.* **2009**, *9* (11), 3945–3948. https://doi.org/10.1021/nl9021623.

(12) Bautista, G.; Dreser, C.; Zang, X.; Kern, D. P.; Kauranen, M.; Fleischer, M. Collective Effects in Second-Harmonic Generation from Plasmonic Oligomers. *Nano Lett.* **2018**, *18* (4), 2571–2580. https://doi.org/10.1021/acs.nanolett.8b00308.

(13) Valev, V. K.; Denkova, D.; Zheng, X.; Kuznetsov, A. I.; Reinhardt, C.; Chichkov, B. N.; Tsutsumanova, G.; Osley, E. J.; Petkov, V.; De Clercq, B.; et al. Plasmon-Enhanced Sub-Wavelength Laser Ablation: Plasmonic Nanojets. *Adv. Mater.* **2012**, *24* (10), OP29-OP35. https://doi.org/10.1002/adma.201103807.

(14) Chen, S.; Li, G.; Zeuner, F.; Wong, W. H.; Pun, E. Y. B.; Zentgraf, T.; Cheah, K. W.; Zhang, S. Symmetry-Selective Third-Harmonic Generation from Plasmonic Metacrystals. *Phys. Rev. Lett.* **2014**, *113* (3), 033901–033905. https://doi.org/10.1103/PhysRevLett.113.033901.

(15) Bautista, G.; Kauranen, M. Vector-Field Nonlinear Microscopy of Nanostructures. *ACS Photonics* **2016**, *3* (8), 1351–1370. https://doi.org/10.1021/acsphotonics.6b00052.

(16) Tai, S.-P.; Wu, Y.; Shieh, D.-B.; Chen, L.-J.; Lin, K.-J.; Yu, C.-H.; Chu, S.-W.; Chang, C.-H.; Shi, X.-Y.; Wen, Y.-C.; et al. Molecular Imaging of Cancer Cells Using Plasmon-Resonant-Enhanced Third-Harmonic-Generation in Silver Nanoparticles. *Adv. Mater.* **2007**, *19* (24), 4520–4523. https://doi.org/10.1002/adma.200602213.

(17) Valev, V. K.; De Clercq, B.; Biris, C. G.; Zheng, X.; Vandendriessche, S.; Hojeij, M.; Denkova, D.; Jeyaram, Y.; Panoiu, N. C.; Ekinci, Y.; et al. Distributing the Optical Near-Field for Efficient Field-Enhancements in Nanostructures. *Adv. Mater.* **2012**, *24* (35), OP208-OP215. https://doi.org/10.1002/adma.201201151.

(18) Valev, V. K.; Baumberg, J. J.; Sibilia, C.; Verbiest, T. Chirality and Chiroptical Effects in Plasmonic Nanostructures: Fundamentals, Recent Progress, and Outlook. *Adv. Mater.* **2013**, *25* (18), 2517–2534. https://doi.org/10.1002/adma.201205178.

(19) Hooper, D. C.; Mark, A. G.; Kuppe, C.; Collins, J. T.; Fischer, P.; Valev, V. K. Strong Rotational Anisotropies Affect Nonlinear Chiral Metamaterials. *Adv. Mater.* **2017**, *29* (13), 1605110–1605116. https://doi.org/10.1002/adma.201605110.

(20) Collins, J. T.; Kuppe, C.; Hooper, D. C.; Sibilia, C.; Centini, M.; Valev, V. K. Chirality and Chiroptical Effects in Metal Nanostructures: Fundamentals and Current Trends. *Adv. Opt. Mater.* **2018**, *6* (2), 1700182. https://doi.org/10.1002/adom.201701345.

(21) Belardini, A.; Larciprete, M. C.; Centini, M.; Fazio, E.; Sibilia, C.; Chiappe, D.; Martella, C.; Toma, A.; Giordano, M.; Buatier de Mongeot, F. Circular Dichroism in the Optical Second-Harmonic Emission of Curved Gold Metal Nanowires. *Phys. Rev. Lett.* **2011**, *107* (25), 257401–257405. https://doi.org/10.1103/PhysRevLett.107.257401.

(22) Valev, V. K.; Silhanek, A. V.; Gillijns, W.; Jeyaram, Y.; Paddubrouskaya, H.; Volodin, A.; Biris, C. G.; Panoiu, N. C.; De Clercq, B.; Ameloot, M.; et al. Plasmons Reveal the Direction of Magnetization in Nickel Nanostructures. *ACS Nano* **2011**, *5* (1), 91–96. https://doi.org/10.1021/nn102852b.

(23) Zheng, W.; Liu, X.; Hanbicki, A. T.; Jonker, B. T.; Lüpke, G. Nonlinear Magneto-Plasmonics. *Opt. Mater. Express* **2015**, *5* (11), 2597–2607. https://doi.org/10.1364/OME.5.002597.

(24) Petralli-Mallow, T.; Wong, T. M.; Byers, J. D.; Yee, H. I.; Hicks, J. M. Circular Dichroism Spectroscopy at Interfaces: A Surface Second Harmonic Generation Study. *J. Phys. Chem.* **1993**, *97* (7), 1383–1388. https://doi.org/10.1021/j100109a022.

(25) Valev, V. K.; Baumberg, J. J.; De Clercq, B.; Braz, N.; Zheng, X.; Osley, E. J.; Vandendriessche, S.; Hojeij, M.; Blejean, C.; Mertens, J.; et al. Nonlinear Superchiral Meta-Surfaces: Tuning Chirality and Disentangling Non-Reciprocity at the Nanoscale. *Adv. Mater.* **2014**, *26* (24), 4074–4081. https://doi.org/10.1002/adma.201401021.

(26) Kruk, S.; Weismann, M.; Bykov, A. Y.; Mamonov, E. A.; Kolmychek, I. A.; Murzina, T.; Panoiu, N. C.; Neshev, D. N.; Kivshar, Y. S. Enhanced Magnetic Second-Harmonic Generation from Resonant Metasurfaces. *ACS Photonics* **2015**, *2* (8), 1007–1012. https://doi.org/10.1021/acsphotonics.5b00215.

(27) Almeida, E.; Shalem, G.; Prior, Y. Subwavelength Nonlinear Phase Control and Anomalous Phase Matching in Plasmonic Metasurfaces. *Nat. Commun.* **2016**, *7*, 10367–

10373. https://doi.org/10.1038/ncomms10367.

(28) Lee, J.; Tymchenko, M.; Argyropoulos, C.; Chen, P. Y.; Lu, F.; Demmerle, F.; Boehm, G.; Amann, M. C.; Alù, A.; Belkin, M. A. Giant Nonlinear Response from Plasmonic Metasurfaces Coupled to Intersubband Transitions. *Nature* **2014**, *511* (7507), 65–69. https://doi.org/10.1038/nature13455.

(29) Li, G.; Zhang, S.; Zentgraf, T. Nonlinear Photonic Metasurfaces. *Nat. Rev. Mater.* **2017**, *2* (5), 17010–17023. https://doi.org/10.1038/natrevmats.2017.10.

(30) Chen, J.; Wang, K.; Long, H.; Han, X.; Hu, H.; Liu, W.; Wang, B.; Lu, P. Tungsten Disulfide–Gold Nanohole Hybrid Metasurfaces for Nonlinear Metalenses in the Visible Region. *Nano Lett.* **2018**, *18* (2), 1344–1350. https://doi.org/10.1021/acs.nanolett.7b05033.

(31) Schlickriede, C.; Waterman, N.; Reineke, B.; Georgi, P.; Li, G.; Zhang, S.; Zentgraf, T. Imaging through Nonlinear Metalens Using Second Harmonic Generation. *Adv. Mater.* **2018**, *30* (8), 1703843–1703849. https://doi.org/10.1002/adma.201703843.

(32) Carron, K. T.; Fluhr, W.; Meier, M.; Wokaun, A.; Lehmann, H. W. Resonances of Two-Dimensional Particle Gratings in Surface-Enhanced Raman Scattering. *J. Opt. Soc. Am. B* **1986**, *3* (3), 430–440. https://doi.org/10.1364/JOSAB.3.000430.

(33) Zou, S.; Schatz, G. C. Narrow Plasmonic/Photonic Extinction and Scattering Line Shapes for One and Two Dimensional Silver Nanoparticle Arrays. *J. Chem. Phys.* **2004**, *121* (24), 12606–12612. https://doi.org/10.1063/1.1826036.

(34) Hicks, E. M.; Zou, S.; Schatz, G. C.; Spears, K. G.; Van Duyne, R. P.; Gunnarsson, L.; Rindzevicius, T.; Kasemo, B.; Käll, M. Controlling Plasmon Line Shapes through Diffractive Coupling in Linear Arrays of Cylindrical Nanoparticles Fabricated by Electron Beam Lithography. *Nano Lett.* **2005**, *5* (6), 1065–1070. https://doi.org/10.1021/nl0505492.

(35) Auguié, B.; Barnes, W. L. Collective Resonances in Gold Nanoparticle Arrays. *Phys. Rev. Lett.* **2008**, *101* (14), 143902. https://doi.org/10.1103/PhysRevLett.101.143902.

(36) Wang, W.; Ramezani, M.; Väkeväinen, A. I.; Törmä, P.; Rivas, J. G.; Odom, T. W. The Rich Photonic World of Plasmonic Nanoparticle Arrays. *Mater. Today* **2018**, *21* (3), 303–314. https://doi.org/10.1016/j.mattod.2017.09.002.

(37) Czaplicki, R.; Kiviniemi, A.; Laukkanen, J.; Lehtolahti, J.; Kuittinen, M.; Kauranen, M. Surface Lattice Resonances in Second-Harmonic Generation from Metasurfaces. *Opt. Lett.* **2016**, *41* (12), 2684–2687. https://doi.org/10.1364/OL.41.002684.

(38) Michaeli, L.; Keren-Zur, S.; Avayu, O.; Suchowski, H.; Ellenbogen, T. Nonlinear Surface Lattice Resonance in Plasmonic Nanoparticle Arrays. *Phys. Rev. Lett.* **2017**, *118* (24), 243904. https://doi.org/10.1103/PhysRevLett.118.243904.

(39) Kravets, V. G.; Schedin, F.; Kabashin, A. V.; Grigorenko, A. N. Sensitivity of Collective Plasmon Modes of Gold Nanoresonators to Local Environment. *Opt. Lett.* **2010**, *35* (7), 956–958. https://doi.org/10.1364/OL.35.000956.

(40) Spackova, B.; Wrobel, P.; Bockova, M.; Homola, J. Optical Biosensors Based on Plasmonic Nanostructures: A Review. *Proc. IEEE* **2016**, *104* (12), 2380–2408. https://doi.org/10.1109/JPROC.2016.2624340.

(41) Gutha, R. R.; Sadeghi, S. M.; Sharp, C.; Wing, W. J. Biological Sensing Using Hybridization Phase of Plasmonic Resonances with Photonic Lattice Modes in Arrays of Gold Nanoantennas. *Nanotechnology* **2017**, *28* (35), 355504. https://doi.org/10.1088/1361-6528/aa7bb5.

(42) Lee, K. S.; El-Sayed, M. A. Gold and Silver Nanoparticles in Sensing and Imaging: Sensitivity of Plasmon Response to Size, Shape, and Metal Composition. *J. Phys. Chem. B* **2006**, *110* (39), 19220–19225. https://doi.org/10.1021/jp062536y.

(43) Kuznetsov, A. I.; Evlyukhin, A. B.; Gonçalves, M. R.; Reinhardt, C.; Koroleva, A.; Arnedillo, M. L.; Kiyan, R.; Marti, O.; Chichkov, B. N. Laser Fabrication of Large-Scale Nanoparticle Arrays for Sensing Applications. *ACS Nano* **2011**, *5* (6), 4843–4849. https://doi.org/10.1021/nn2009112.

(44) Svedendahl, M.; Chen, S.; Dmitriev, A.; Käll, M. Refractometric Sensing Using Propagating versus Localized Surface Plasmons: A Direct Comparison. *Nano Lett.* **2009**, *9* (12), 4428–4433. https://doi.org/10.1021/nl902721z.

(45) Offermans, P.; Schaafsma, M. C.; Rodriguez, S. R. K.; Zhang, Y.; Crego-Calama, M.; Brongersma, S. H.; Gómez Rivas, J. Universal Scaling of the Figure of Merit of Plasmonic Sensors. *ACS Nano* **2011**, *5* (6), 5151–5157. https://doi.org/10.1021/nn201227b.

(46) Špačková, B.; Homola, J. Sensing Properties of Lattice Resonances of 2D Metal Nanoparticle Arrays: An Analytical Model. *Opt. Express* **2013**, *21* (22), 27490–27502. https://doi.org/10.1364/OE.21.027490.

(47) Zou, S.; Janel, N.; Schatz, G. C. Silver Nanoparticle Array Structures That Produce Remarkably Narrow Plasmon Lineshapes. *J. Chem. Phys.* **2004**, *120* (23), 10871–10875. https://doi.org/10.1063/1.1760740.

(48) Markel, V. A. Comment on "Silver Nanoparticle Array Structures That Produce Remarkably Narrow Plasmon Line Shapes" [J. Chem. Phys. 120, 10871 (2004)]. *J. Chem. Phys.* **2005**, *122* (9), 097101. https://doi.org/10.1063/1.1859281.

(49) Zou, S.; Schatz, G. C. Response to "Comment on 'Silver Nanoparticle Array Structures That Produce Remarkable Narrow Plasmon Line Shapes' " [J. Chem. Phys. 120, 10871 (2004)]. *J. Chem. Phys.* **2004**, *122* (9), 097102. https://doi.org/10.1063/1.1859282.

(50) Li, J.; Ye, J.; Chen, C.; Li, Y.; Verellen, N.; Moshchalkov, V. V.; Lagae, L.; Van Dorpe, P.

Revisiting the Surface Sensitivity of Nanoplasmonic Biosensors. *ACS Photonics* **2015**, *2* (3), 425–431. https://doi.org/10.1021/ph5004779.

(51) Wang, D.; Bourgeois, M. R.; Lee, W. K.; Li, R.; Trivedi, D.; Knudson, M. P.; Wang, W.; Schatz, G. C.; Odom, T. W. Stretchable Nanolasing from Hybrid Quadrupole Plasmons. *Nano Lett.* **2018**, *18* (7), 4549–4555. https://doi.org/10.1021/acs.nanolett.8b01774.

(52) Butet, J.; Bachelier, G.; Russier-Antoine, I.; Jonin, C.; Benichou, E.; Brevet, P. F. Interference between Selected Dipoles and Octupoles in the Optical Second-Harmonic Generation from Spherical Gold Nanoparticles. *Phys. Rev. Lett.* **2010**, *105* (7), 077401. https://doi.org/10.1103/PhysRevLett.105.077401.

(53) Nappa, J.; Russier-Antoine, I.; Benichou, E.; Jonin, C.; Brevet, P. F. Wavelength Dependence of the Retardation Effects in Silver Nanoparticles Followed by Polarization Resolved Hyper Rayleigh Scattering. *Chem. Phys. Lett.* **2005**, *415* (4–6), 246–250. https://doi.org/10.1016/j.cplett.2005.08.143.

(54) Nappa, J.; Russier-Antoine, I.; Benichou, E.; Jonin, C.; Brevet, P. F. Second Harmonic Generation from Small Gold Metallic Particles: From the Dipolar to the Quadrupolar Response. *J. Chem. Phys.* **2006**, *125* (18), 184712. https://doi.org/10.1063/1.2375095.

(55) Bachelier, G.; Butet, J.; Russier-Antoine, I.; Jonin, C.; Benichou, E.; Brevet, P.-F. Origin of Optical Second-Harmonic Generation in Spherical Gold Nanoparticles: Local Surface and Nonlocal Bulk Contributions. *Phys. Rev. B Condens. Matter Mater. Phys.* **2010**, *82* (23), 235403. https://doi.org/10.1103/PhysRevB.82.235403.

(56) Evlyukhin, A. B.; Reinhardt, C.; Zywietz, U.; Chichkov, B. N. Collective Resonances in Metal Nanoparticle Arrays with Dipole-Quadrupole Interactions. *Phys. Rev. B Condens. Matter Mater. Phys.* **2012**, *85* (24), 245411. https://doi.org/10.1103/PhysRevB.85.245411.

(57) Russier-Antoine, I.; Benichou, E.; Bachelier, G.; Jonin, C.; Brevet, P. F. Multipolar Contributions of the Second Harmonic Generation from Silver and Gold Nanoparticles. *J. Phys. Chem. C* **2007**, *111* (26), 9044–9048. https://doi.org/10.1021/jp0675025.

(58) Smirnova, D.; Kivshar, Y. S. Multipolar Nonlinear Nanophotonics. *Optica* **2016**, *3* (11), 1241–1255. https://doi.org/10.1364/OPTICA.3.001241.

(59) Timbrell, D.; You, J. W.; Kivshar, Y. S.; Panoiu, N. C. A Comparative Analysis of Surface and Bulk Contributions to Second-Harmonic Generation in Centrosymmetric Nanoparticles. *Sci. Rep.* **2018**, *8* (1), 3586. https://doi.org/10.1038/s41598-018-21850-8.

(60) Lumerical Inc. Http://Www.Lumerical.Com/Tcad-Products/Fdtd/.

(61) Dadap, J. I.; Shan, J.; Heinz, T. F. Theory of Optical Second-Harmonic Generation from a Sphere of Centrosymmetric Material: Small-Particle Limit. *J. Opt. Soc. Am. B* **2004**, *21* (7), 1328–1347. https://doi.org/10.1364/JOSAB.21.001328.

(62) Butcher, P.; Cotter, D. *The Elements of Nonlinear Optics*; Cambridge University Press, **1990**.

(63) Vecchi, G.; Giannini, V.; Gómez Rivas, J. Shaping the Fluorescent Emission by Lattice Resonances in Plasmonic Crystals of Nanoantennas. *Phys. Rev. Lett.* **2009**, *102* (14), 146807. https://doi.org/10.1103/PhysRevLett.102.146807.

(64) Green, R. J.; Frazier, R. A.; Shakesheff, K. M.; Davies, M. C.; Roberts, C. J.; Tendler, S. J. B. Surface Plasmon Resonance Analysis of Dynamic Biological Interactions with Biomaterials. *Biomaterials* **2000**, *21* (18), 1823–1835. https://doi.org/10.1016/S0142-9612(00)00077-6.

(65) Huttunen, M. J.; Rasekh, P.; Boyd, R. W.; Dolgaleva, K. Using Surface Lattice Resonances to Engineer Nonlinear Optical Processes in Metal Nanoparticle Arrays. *Phys. Rev. A* **2018**, *97* (5), 053817. https://doi.org/10.1103/PhysRevA.97.053817.

(66) Belardini, A.; Centini, M.; Leahu, G.; Hooper, D. C.; Li Voti, R.; Fazio, E.; Haus, J. W.; Sarangan, A.; Valev, V. K.; Sibilia, C. Chiral Light Intrinsically Couples to Extrinsic/Pseudo-Chiral Metasurfaces Made of Tilted Gold Nanowires. *Sci. Rep.* **2016**, *6* (1), 31796. https://doi.org/10.1038/srep31796.

(67) Aouani, H.; Navarro-Cia, M.; Rahmani, M.; Sidiropoulos, T. P. H. H.; Hong, M.; Oulton, R. F.; Maier, S. A. Multiresonant Broadband Optical Antennas As Efficient Tunable Nanosources of Second Harmonic Light. *Nano Lett.* **2012**, *12* (9), 4997–5002. https://doi.org/10.1021/nl302665m.

(68) Zhang, Y.; Grady, N. K.; Ayala-Orozco, C.; Halas, N. J. Three-Dimensional Nanostructures as Highly Efficient Generators of Second Harmonic Light. *Nano Lett.* **2011**, *11* (12), 5519–5523. https://doi.org/10.1021/nl2033602.

(69) Dong, Z.; Asbahi, M.; Lin, J.; Zhu, D.; Wang, Y. M.; Hippalgaonkar, K.; Chu, H. S.; Goh, W. P.; Wang, F.; Huang, Z.; et al. Second-Harmonic Generation from Sub-5 Nm Gaps by Directed Self-Assembly of Nanoparticles onto Template-Stripped Gold Substrates. *Nano Lett.* **2015**, *15* (9), 5976–5981. https://doi.org/10.1021/acs.nanolett.5b02109.

(70) Guyot-Sionnest, P.; Shen, Y. R. Bulk Contribution in Surface Second-Harmonic Generation. *Phys. Rev. B Condens. Matter Mater. Phys.* **1988**, *38* (12), 7985–7989. https://doi.org/10.1103/PhysRevB.38.7985.

(71) Bachelier, G.; Russier-Antoine, I.; Benichou, E.; Jonin, C.; Brevet, P.-F. Multipolar Second-Harmonic Generation in Noble Metal Nanoparticles. *J. Opt. Soc. Am. B* **2008**, *25* (6), 955–960. https://doi.org/10.1364/JOSAB.25.000955.

(72) Nappa, J.; Revillod, G.; Russier-Antoine, I.; Benichou, E.; Jonin, C.; Brevet, P. F. Electric Dipole Origin of the Second Harmonic Generation of Small Metallic Particles. *Phys. Rev. B* **2005**, *71* (16), 165407. https://doi.org/10.1103/PhysRevB.71.165407.

(73) Li, J.; Ye, J.; Chen, C.; Hermans, L.; Verellen, N.; Ryken, J.; Jans, H.; Van Roy, W.; Moshchalkov, V. V.; Lagae, L.; et al. Biosensing Using Diffractively Coupled Plasmonic Crystals: The Figure of Merit Revisited. *Adv. Opt. Mater.* **2015**, *3* (2), 176–181. https://doi.org/10.1002/adom.201400394.

(74) Sadeghi, S. M.; Wing, W. J.; Campbell, Q. Normal and Anomalous Plasmonic Lattice Modes of Gold Nanodisk Arrays in Inhomogeneous Media. *J. Appl. Phys.* **2016**, *119* (11), 114307. https://doi.org/10.1063/1.4944324.

ToC Figure